Anomalously large spectral shifts near the quantum tunnelling limit in plasmonic rulers with subatomic resolution

Charlie Readman[1,2], Bart de Nijs[1], István Szabó[3], Angela Demetriadou[4], Ryan Greenhalgh[1,5], Colm Durkan[5], Edina Rosta[3], Oren A. Scherman*[2], and Jeremy J. Baumberg*[1]

[1] NanoPhotonics Centre, Cavendish Laboratory, Department of Physics, JJ Thompson Avenue, University of Cambridge, Cambridge, CB3 0HE, UK

[2] Melville Laboratory for Polymer Synthesis, Department of Chemistry, University of Cambridge, Lensfield Road, Cambridge CB2 1EW, UK

[3] Department of Chemistry, King's College London, 7 Trinity Street, London SE1 1DB, United Kingdom

[4] School of Physics and Astronomy, University of Birmingham, Edgbaston, Birmingham, B15 2TT, UK

[5] The Nanoscience Centre, 11 JJ Thompson Avenue, University of Cambridge, Cambridge, CB3 0FF, UK

ABSTRACT

The resonance wavelength of a coupled plasmonic system is extremely sensitive to the distance between its metallic surfaces, resulting in 'plasmon rulers'. We explore this behaviour in the sub-nm regime using self-assembled monolayers of bis-phthalocyanine molecules in a nanoparticle-on-mirror (NPoM) construct. These allow unprecedented sub-angstrom control over spacer thickness via choice of metal centre, in a gap-size regime at the quantum-mechanical limit of plasmonic enhancement. A dramatic shift in the coupled plasmon resonance is observed as the gap size is varied from 0.39 to 0.41 nm. Existing theoretical models are unable to account for the observed spectral tuning, which requires inclusion of the quantum-classical interface, emphasising the need for new treatments of light at the sub-nanoscale.

KEYWORDS: Nanocavities, Quantum Plasmonics, Phthalocyanines, Nano-assembly, DFT, and SERS.

Introduction

Placing two noble metal nanostructures a short distance (< 10 nm) from each other leads to electronic coupling of the collective electron oscillations (plasmons). This coupling creates a tightly-confined, redshifted and enhanced optical field within the interparticle gap, whose resonance wavelength depends strongly on the local environment.[1–3] This sensitivity has already led to applications in chemical and biological sensing[4–6], as well as electronic devices.[7–10] One key implementation has been the plasmon ruler,[11–16] in which the resonant wavelength of such a coupled system shifts predictably as the interparticle spacing (d) is varied, leading to length measurements with a much larger interaction range, longer lifetime, and greater robustness than using fluorescence resonant energy transfer (FRET).[17–19]

Plasmon rulers have been studied both experimentally[15,20,21] and theoretically[1,13,14,22] at a range of length scales. For gap sizes d > 1 nm the dimer response can be numerically predicted using Maxwell's equations**,** in good agreement with experiments.[1,15,23] Simplified analytical models also exist[1,24,25] as well as empirical 'universal' plasmon ruler equations[11–14] that can be modified with further exponential terms to account for smaller gaps.[16] However, these models fail to describe systems with $d \lesssim 0.5$ nm, at which point electron nonlocality and spillout become significant.[1,21,26–30]

For sub-nm gaps, this non-classical behaviour leads to a reduction or even reversal of the observed redshift with decreasing gap size.[1,21,31–33] The inherent nonlocality of electrons is accounted for with hydrodynamic terms in simplified coupling models. Electron spillout beyond the notionally-sharp metal interface arises from Coulomb repulsion and electron degeneracy pressure, which can be modelled with time-dependent density functional theory (TD-DFT). Full quantum treatment however, can only currently be implemented for small (< 5 nm diameter) nanoparticles or clusters and only for simple metals like Na.[31,34–36] Additionally, for gaps within the quantum regime, $d_{QM} \approx \ln(3q\lambda\alpha/2\pi) \approx$ 0.4 nm, the electron tunnelling across the gap counteracts the charge buildup on either side, diminishing the red-shifts of plasmon resonant wavelength λ; here $\alpha = 1/137$ is the fine structure constant, and the semiclassical electron tunnelling wavenumber $q = \sqrt{2m\phi}/\hbar$ = 11 nm^{-1} for work-function of Au $\phi = 4.8$ eV.[21,27,36,37]

Despite a comprehensive focus on developing theoretical models of the quantum plasmonic regime, the number of experiments remains extremely limited. This is due to the difficulty of reliable control at such sub-nm length scales, as well as the problem of independent measurement of such gap sizes. Top-down lithographic approaches reach only down to ~5nm before suffering from extreme irreproducibility,[12,19,38] while STM approaches are hard to combine with optics and unstable in ambient conditions.[21,39,40] Bottom-up assembly typically aims for plasmonic dimers with molecular control of the gap. A standard approach has been to use self-assembled monolayers (SAMs) of alkanethiols, the known length of which allows fine control over the spacing,[1,15,20,41] in theory creating gaps down to ~0.5 nm. However there remains little agreement over precisely when quantum effects become important in this plasmonic gap ruler.[19,33]

To address the quantum regime more reliably, we introduce here a new class of bis-phthalocyanine (BPc) plasmonic spacers capable of fine tuning the gap size between 0.39-0.41 nm around the quantum length scale d_{QM}.[42–47] These molecular spacers are sandwich complexes consisting of a central lanthanide ion and two conjugated phthalocyanine (Pc) ligands in close proximity (Figure 1a). The BPc electronic structure is dominated by the resultant $\pi - \pi$ coupling.[42,47–53] In comparison to the previous use of graphene[2,54] as a spacer, which has a nominal 0.34 nm thickness, these BPc-based systems are stable against Au-Au van der Waals forces, physically and chemically robust, and highly suited to testing out models of conduction at optical frequencies. It also introduces a new degree of freedom into the gap, since the coupled Pc_2 ligand pair is easily oxidised and reduced,[47,55–59] modifying the gap electromagnetic properties. We show that the resulting plasmonic constructs are robust, scalable and easy to fabricate via bottom-up nano-assembly. They also provide the smallest easily constructed stable nano-resonators, with volumes $V_I \sim Dd^2/n_g^2 \sim 6$ nm^3.[24] We then show that existing theoretical models cannot account for the spectral tuning of the mode with such gap sizes.

This confirms the need for theories that treat coupled image dipoles and electromagnetic resonances of plasmonic metallic environments containing complex, redox-active molecules with large numbers of electrons. This also highlights the problems posed by the quantum-classical interface.

Experimental

While dimers are the simplest model system, they remain challenging to create in high yield (since larger-scale aggregates generally form).[5,60] As a result we adopt a comparably simple geometry termed the nanoparticle-on-mirror (NPoM) system, in which the partner nanoparticle (NP) is replaced by a flat plasmonic surface creating analogous image charges and dipoles (Figure 1b).[2,24,61] The tightly coupled charges either side of the gap create red-shifted coupled plasmon modes, whose spectral position is extremely sensitive to the size (d) and refractive index (n_g) of the gap.[2,24]

In the dark-field scattering spectrum of a typical NPoM construct (Figure 1e) using AuNPs of diameter D = 80 nm, two distinct plasmonic resonances are observed. First is the transverse (T) mode excited by light polarised parallel to the surface, which is located at wavelength $\lambda_T \approx 533$ nm and is barely perturbed by the properties of the spacer (because the light is concentrated outside this layer). The second, coupled (C) mode is red-shifted due to the interaction with image charges on each gap surface and is tightly confined to the nanocavity. Both the peak wavelength of the coupled resonance (λ_C) and the C/T intensity ratio (I_r) depend strongly upon the physical properties of the gap spacer, including its conductance (G); an increase in d or G causes the C mode to blue shift, while an increase in n_g leads to a red shift.[2,24,61] This sensitivity allows us to explore the optical effects of incorporating a series of BPc derivatives as NPoM molecular spacers. The BPc compounds studied here are $LnPc^*_2$ (hereafter referred to as BPc*), where the lanthanide Ln = {Sm, Tb, Er, Lu} and Pc* denotes a phthalocyanine ligand octa-peripherally substituted with *n*-dodecylthio groups (Figure 1a) to improve solubility and encourage self-assembly on the Au surface.[45,62,63]

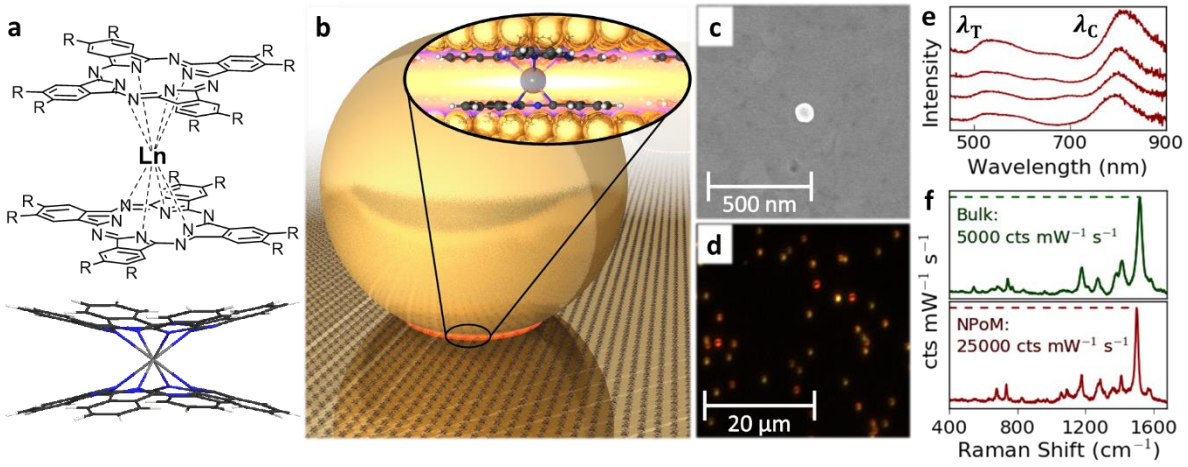

Figure 1. (**a**) Top: BPc* chemical structure. Ln = {Sm, Tb, Er, Lu}, R = $S^nC_{12}H_{25}$. Bottom: geometry optimised (DFT) stick model of $LuPc_2$ with C (black), H (white), N (blue), Ln (grey), and R groups omitted for clarity. (**b**) Schematic of 80 nm NPoM on a full BPc* monolayer (R groups omitted). Inset shows side-view of BPc molecules in NPoM cavity. (**c**) SEM image of single NPoM. (**d**) Optical dark-field (DF) image of an $ErPc^*_2$ NPoM sample. (**e**) Individual NPoM DF spectra (normalised, offset). (**f**) Top: Raman spectrum of $ErPc^*_2$. Bottom: SERS spectrum of a single $ErPc^*_2$ NPoM.

Results

To confirm successful assembly of these constructs (see Materials & Methods) with hotspots (Figure 1b) containing BPc* molecules, isolated NPoMs are analysed with scanning electron microscopy (SEM), surface-enhanced Raman spectroscopy (SERS) and dark field (DF) scattering spectroscopy. SEM images (Figure 1c) reveal isolated individual NPoMs with nearest-neighbour distances larger than the optical collection spot size (~1 µm). Significant lateral coupling between NPs is not observed at these separation distances,[13,16] so all plasmonic coupling observed is due to NP-surface interactions. Individually resolved NPoMs can be viewed under DF (Figure 1d), with each individual NPoM DF

spectrum containing a single sharp near-infrared coupled resonance (Figure 1e). NP aggregates and NPoMs too close to be distinguished are detected and removed during post-processing of the spectra. Comparison of NPoM SERS spectra (Figure 1f, bottom) with Raman spectra of bulk $LnPc^*_2$ (Fig 1f, top) demonstrates the presence of BPc* in the optical hotspot of the nanogap. No SERS is observed when the laser is displaced off the NPoM. The combination of plasmonic field enhancement (see below) and resonant Raman effects (since BPc* has an electronic resonance around 600-700 nm[50,64]) leads to signals of ~25000 cts mW^{-1} s^{-1} from a single NPoM, which is large enough to enable fast dynamic SERS.

Assuming $\leq$ 100% surface coverage and a planar-lattice molecular separation of ~3.0 nm,[62] we estimate a population of $\leq$ 95 BPc* molecules within each NPoM gap. The estimated lateral spatial intensity full-width half-maximum of the confined optical field is $\Delta x = \sqrt{Dd}/n_g$.[21] This corresponds to ~4 nm for nanoparticle diameters D = 80 nm, giving an average of 10-15 BPc* molecules probed within each NPoM hotspot. This implies that SERS emission of ~2500 cts mW^{-1} s^{-1} from each molecule is achieved in this NPoM, more than in any other system yet observed. Depending on preparation and measurement conditions, statistical variation in surface coverage will lead to significant lateral variations in the physical properties of the SAM (such as n_g) at this length scale,[40,65] with Poissonian error of $\pm$35%. The AuNP shape/size polydispersity is also expected to cause variations in plasmonic coupling behaviour across such samples.[2,61,66] This inherent variability for single nano-objects thus leads to an approximately normal distribution for λ_C.

To account for this variation, measurements of dark field scattering spectra are collected from approximately 1000 NPoMs for each sample (Figure 2a); a vertical z-stack is performed in each case to correct for chromatic aberration.[2] Individual spectra are analysed using a multi-peak fit algorithm and spectra containing more than one coupled plasmon resonance excluded to minimise the influence of significantly non-spherical particles.[2,54] The spectral range 450-900 nm is then divided into 80 bins (each 5.7 nm wide) and individual spectra sorted into these according to λ_C (Figure 2a, bottom). As observed previously,[2] the sharp coupled mode resonance persists when averaging the contents of each bin (Figure 2a, top), yielding highly reproducible representative spectra with high signal-to-noise ratio. The binned frequency distribution of a sample of 1000 NPoMs typically gives a narrow Gaussian profile (Figure 2a, bottom), and the centre of this gives $\bar{\lambda}_C$.

The measured $\bar{\lambda}_C$ values of 760-810 nm for samples with different Ln imply nanoparticle-surface separations of < 1 nm for reasonable estimates of $n_g \approx 1.5$, based on organic monolayers.[67,68] This confirms that only a single (sub)monolayer of BPc molecules is found in the gap, consistent with existing literature, in which STM measurements mostly reveal arrangements of BPc derivatives with Pc planes parallel to the surface and apparent height ~0.4nm.[45,62,63,69–71] Based on DFT calculations (See supporting information (SI) for details) and literature data,[42–44,46,47] we thus expect NP-surface separations in the range $0.3 < d < 0.5$ nm.

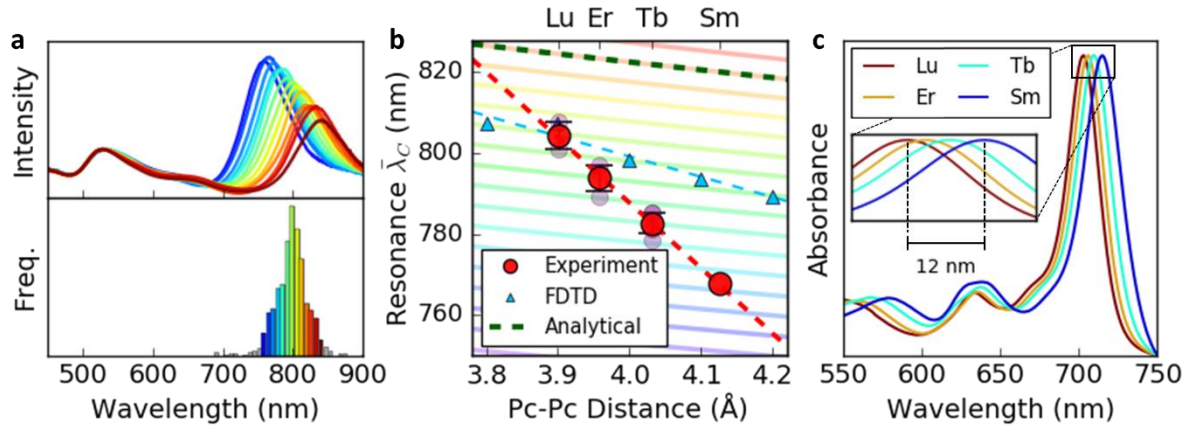

Figure 2. (**a**) Typical NPoM DF spectra λ_C distribution (here for ErPc*$_2$). Individual DF spectra (top) are averages of all spectra in each histogram bin of corresponding colour (bottom). (**b**) Shift in $\bar{\lambda}_C$ with increasing size of NPoM spacer (from DFT calculations). Red circles represent average measured $\bar{\lambda}_C$ for each Ln centre (individual samples are purple circles, each of 100 – 2000 spectra); error bars show standard deviation between samples. Solid lines show calculated shift in $\bar{\lambda}_C$ with increasing spacer thickness (using analytical model from Ref. 24) for $1.10 \leq n_g \leq 1.55$ ($n_g = 1.5$, green dashed line). Finite-difference time domain (FDTD) simulations are blue triangles. (**c**) UV-Vis absorbance spectra of BPc* (10 μM in $CHCl_3$) illustrating shift in λ_α.

We first correlate these systematic spectral shifts in the dark field scattering spectra with the expected thickness of the BPc* gap as the Ln core is exchanged. DFT calculations (SI) show a slight decrease in average Pc-Pc distance (estimated as in Ref. 43) with increasing Ln atomic number (Z_{Ln}) for Sm → Lu. As expected, the corresponding NPoMs exhibit a redshift in $\bar{\lambda}_C$ for Sm → Lu (Figure 2b). However, both classical analytical[24] and finite-difference time domain (FDTD) calculations (Materials & Methods) suggest the slight difference in expected gap size ($\Delta d \approx 0.02$ nm) is far too small to account for the >35 nm (~70 meV) shift in $\bar{\lambda}_C$. This robust result is the key finding here, which demands a more sophisticated understanding.

Effect of Molecular Structure

The results presented here suggest deviations from classical behaviour, which is indeed expected at this length scale (as discussed above). However, it is also important to consider changes in molecular properties other than height as Z_{Ln} is varied. As previously described, conductance, refractive index/polarizability, and charge transfer all influence the plasmon coupling behaviour.[2,72]

BPc derivatives are strong visible light absorbers[49,73,74] and in such tightly-confined plasmonic NPoM systems, strong coupling has already been observed for dyes.[72] While the UV-Vis absorption spectra of the BPc* complexes studied here exhibit a noticeable spectral shift from Sm to Lu (Figure 2c), the range $\Delta\lambda_\alpha \approx 12$ nm ($\Delta\nu \approx 30$ meV) is only 40% of the observed energy shift in $\bar{\lambda}_C$ and occurs in the opposite direction. The corresponding resonant refractive index is larger on the longer wavelength side of λ_α, and a quantitative model based on the measured $n_g(\lambda)$ for $TbPc_2$ thin films[67], shifted according to $\lambda_\alpha(\mathrm{Ln})$, indeed confirms that this cannot account for $\Delta\lambda_C$ (Figs.S2-5 and accompanying discussion). The predicted increase in n_g from Lu to Sm at the plasmon resonance decreases $\Delta\lambda_C$ relative to the model, directly contradicted by our experimental data.

Due to the mismatch in energy and symmetry between the Ln 4*f* valence orbitals and those of the ligand(s) in rare earth element complexes,[42,75] Ln ions tend to behave chemically as hard ionic spheres. Because of this, the electronic structure of the BPc* complexes stems primarily from Pc-Pc

orbital overlap, which is extremely sensitive to interplanar distance and skew angle θ, the relative twist between the top and bottom Pc molecules (Figure 3a).[42,47,51,76] While preliminary DFT calculations (SI) and literature data[43,47,52] suggest a staggered molecular conformation ($\theta = 45°$) in the neutral state, θ has been observed to vary with Ln size in singly-reduced $[BPc]^-$ complexes.[43,67,77] Previous studies also suggest that BPc derivatives can adopt this reduced state upon contact with a metal surface.[76,78,79] Subsequent variations in θ may therefore affect the molecular polarizability and conductance.[42,51]

To investigate this hypothesis, both the energy and polarisability (z-component, parallel to the optical field in this NPoM C mode) of unsubstituted BPc molecules (Ln = Sm, Tb, Er, Lu) were calculated using DFT for a range of skew angles from 0 to 45° (Figure 3a,b. See SI for details). The overall energy barrier for rotation decreases with increasing Ln size, as expected (Figure 3b, top), due to a decrease in steric hindrance. While single-electron reduction lowers this barrier slightly, an energy minimum still exists at or near $\theta = 45°$ in all cases. The lowest activation barrier (210 meV ≈ 5 kcal/mol for $[SmPc_2]^-$) is an order of magnitude higher than the available thermal energy at room temperature (25 meV = 0.593 kcal mol^{-1} at 298 K).

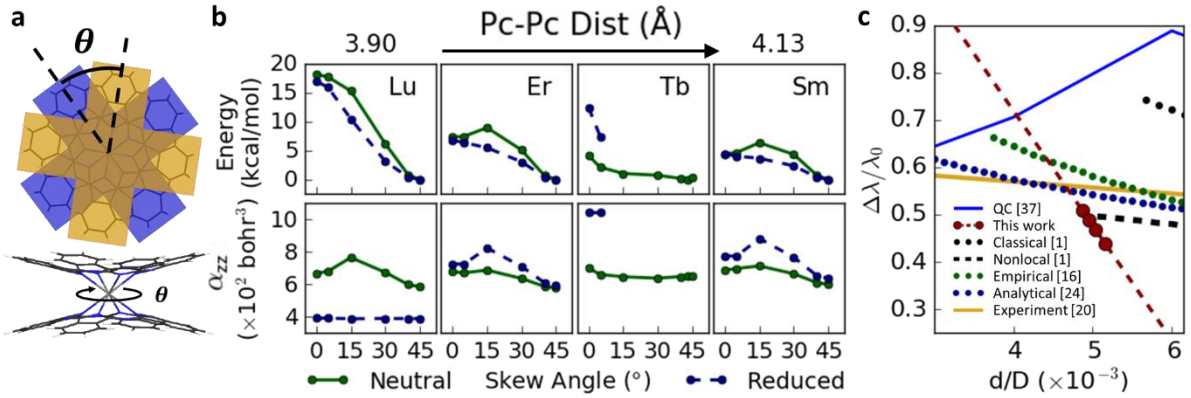

Figure 3. (**a**) Schematic of BPc molecule illustrating skew angle θ. (**b**) Variation in relative energy (top) and polarizability (bottom) with change in skew angle for $LnPc_2$ and $LnPc_2^-$ (Ln = Lu, Er, Tb, Sm). (**c**) Comparison of selected models from Table 1. QC = quantum corrected.

While local heating in the gap might provide energy to overcome this barrier, the calculations also show a polarizability minimum at 45°, and a maximum between 15° and 30°, as well as an overall increase in polarizability (and hence n_g) with increasing Ln size/interplanar distance (Figure 3b, bottom). If these differences in θ and molecular polarizability were then to significantly affect the plasmon resonance, $\Delta\bar{\lambda}_C$ would be even smaller than that predicted by our simulations, which is the opposite of the experimental trend observed (Figure 2b).

Another consequence of the proximity of BPc is the possibility of local electron redistribution at the Au surface. Slight differences in frontier orbital energies (Fig. S6) may affect the charging behaviour of adsorbed BPc molecules and through electrostatic interactions, the local electron density could be affected. This would in turn affect the local plasma frequency near the gap and cause a slight shift in λ_C. A slight decrease in energy of the lowest unoccupied molecular spin orbital is observed, which is expected to have a redshifting effect from Lu to Sm (see SI for further discussion). Again, this is the opposite of the trend we observe. Interpretation of the result is further complicated by hybridisation between BPc and Au electronic states,[78] which is beyond the scope here, but pertinent to effects in this sub-nm gap regime.

For variations in molecular conductance to cause the anomalous shift in $\bar{\lambda}_C$, an increase in conductance with Ln size would be required. To test this, analytical calculations were performed using the model of Benz *et al*.[24], with conductance allowed to vary as a polynomial function of gap size, for a range of refractive index and inductance values. All scenarios require conductances on the order of $10^8 - 10^9\ G_0$. While BPc is known to exhibit (semi)conducting behaviour,[55,64,69] most studies focus on DC conductance of BPc thin films or long molecular wires. This is not directly comparable to an NPoM system with a junction of single-molecule thickness, in which the relevant property is AC conductance at optical frequencies. Any conductance exhibited due to BPc semiconductivity/redox will occur at much longer timescales than optical periods of a few fs and therefore have little effect on λ_C. This is confirmed by Noda *et al*.[80] who observed behaviour consistent with a tunneling mechanism during electrical measurements of BPc:AuNP aggregates (Ln = Tb, Lu), implying negligible conductivity ($\ll G_0$) of the molecular junctions. Conductance effects are thus not considered further as the cause of the observed λ_C tuning.

Deviation from Classical Behaviour

Having eliminated molecular contributions to the $\bar{\lambda}_C$ shift, more subtle consequences of gap size variation are the most probable cause, including non-classical effects. Models employing classical electrodynamics predict a shift of $\bar{\lambda}_C \to \infty$ as $d \to 0$.[13,22] While this works for larger separations ($d >$ 2 nm), the classical treatment fails to correctly predict coupling behaviours at smaller distances.[1] The main reasons are electron nonlocality and spillout, both of which suppress the plasmon in the gap. Solution of the quantum wavefunctions of electrons show that Coulomb repulsion and Fermi pressures lead to spatial dispersion of electrons as gap sizes become comparable to the electron density decay length. A purely local treatment of the system is therefore no longer applicable.[1,21,31–33] Experiments performed in this regime show a broadening of the coupled plasmon resonance peak and a decrease in magnitude of $\Delta\bar{\lambda}_C$ as d decreases.[1,15,21] However, we emphasise once again that, in this work, the opposite is experimentally observed.

Due to the very small distance range explored here ($\Delta d \approx$ 0.02 nm), electron nonlocality is unlikely to cause much variation in the spectral shift. However, quantum tunnelling becomes important for $d <$ 0.5 nm.[19,21,81] As the gap sizes explored here probe the upper bounds of this tunnelling regime, electron spillout is likely to change much more dramatically with d at this length scale. Tunelling currents effectively increase the gap conductance at smaller separations, leading to a screening of the coupled plasmon mode.[24,37,61] However as with the appearance of nonlocal effects, a *decrease* in the magnitude of the λ_C redshift and field enhancement is then expected, followed by a complete reversal and λ_C blueshift.[21,36,37]

A range of numerical[1,21,22,82] and analytical[1,24,35,83] models incorporating nonlocality[30,82,83] and quantum corrections for electron tunnelling[31,34–37] have already been developed. Nonlocal models often include hydrodynamic treatment of the electron gas,[1,30,81] while the quantum corrected model (QCM) accounts for electron tunnelling using TDDFT calculations.[1,34–36] When considering the latter, nanostructures of the dimensions explored in this paper ($D =$ 80 nm) are still far too computationally expensive to perform a full quantum calculation. Small clusters, jellium models and/or simpler metals like Na are therefore used.

Table 1 and Figure 3c outline theoretical and experimental data from the literature that is relevant to our system. Although the data comes from a range of different NP sizes, scaling allows

suitable comparison:[13,16] using normalisation of $\bar{\lambda}_C$ to λ_T and of d to D allows extraction of the tuning rate $\eta = \frac{d\lambda_r}{dx}$, where $\lambda_r \approx \bar{\lambda}_C/\lambda_T - 1$ and $x = 2d/D$.

Table 1. Comparison of relevant literature data exploring the normalised $\bar{\lambda}_C$ tuning rate in the sub-nm gap regime. *a* = AuNP/sphere dimer; *b* = Au NPoM.

Method	**Tuning rate η (at d/D = 0.005)**	**NP Size (nm)**	**Gap Size (nm)**	**Gap n_g**	**Reference**
Local[a]	-14.5	D = 120	$0.1 \leq d \leq 10$	1	22
Local[a]	-7.1	D = 20	$0.1 \leq d \leq \infty$	1	[82]
Nonlocal[a]	-3.8				
Local[b]	-37.6	D = 60	$0.3 \leq d \leq 20$	1.8	1
Nonlocal/expt[b]	-5.8				
Local[a]	-17.0	D = 50	$0 \leq d \leq 1.5$	1	37
QC[a]	+45.6				
Expt[b]	-11.4	D = 60	$0.5 \leq d \leq 30$	1.8	15
Expt[b]	-8.2	D = 60	$0.7 \leq d \leq 1.6$	1.8	20
Local[b]	-6.0	D = 60	$0.5 \leq d \leq 1.6$	1.8	41
QC[b]	-5.6				
Expt[b]	-7.3				
Local[a]	-27.7	Various	Various	1.33	16
Expt[b]	**-121**	**D = 80**	**$0.39 \leq d \leq 0.41$**	**1.5**	**This work**
Local[b]	-57.9				
Semi-local[b]	-19.8				

As predicted, nonlocal and/or quantum corrections of these coupled plasmonic systems lead to smaller values of η, which is contrary to the data presented in this work. At a gap spacing of 0.4 nm ($x = 0.01$ for $D = 80$ nm) we see relative shifts in $\bar{\lambda}_C$ that are an order of magnitude larger than tuning rates predicted even by 'unrealistic' classical local models.

It is worth noting that no previously published experimental realisations of these systems have more than one data point below ~0.5 nm (if any), nor do they have such fine control over the gap thickness as the tunnelling regime is reached. Sub-nm plasmonic rulers explored thus far in the literature often rely on very few data points in the sub-nm range and extrapolate from larger distances. The highly-redshifted coupled mode we observe suggests that previous estimates of gaps for alkanethiols are incorrect, and that they change their surface configuration when exposed to the large compressive van-der-Waals forces inside such nanogaps. While Savage *et al.*[21] explore this regime with a Au AFM tip dimer, the AuNP sizes involved ($D \approx 300$ nm) are significantly larger than those explored here and the tunnelling regime is approached differently, requiring applied force to displace trapped water molecules and achieve full metallic contact. So far, anomalous spectral shifts of this magnitude have not been observed. In a simple model of tunnelling through a vacuum gap, the conductivity is given by $\sigma \propto \exp\{-2qd\} = \exp\{-d/0.045\ \text{nm}\}$;[21] the corresponding fractional change in tunnelling conductivity for $\Delta d \approx 0.02$ nm is $\Delta\sigma/\sigma \sim \exp\{-0.02/0.045\} = 0.64$. A simple estimate of how this would affect the plasmon coupled mode around the critical conductance from Ref. 61 is given by $\frac{\partial \lambda_C}{\partial(\sigma/G_0)} = 40$ nm, suggesting shifts of $\Delta\lambda_C = 26$ nm. Although this is comparable to

the shift observed in our experiments, we again note that the sign of the effect is reversed; quantum tunnelling would be expected to reduce, rather than increase, the tuning rate within this regime. We are thus forced to conclude that in such planar conducting molecular systems in plasmonic gaps in the quantum regime, there are new effects not yet predicted by any theoretical model.

The implication of our work suggests caution is needed when exploring the applicability of nm-scale plasmon rulers. When investigating the response of coupled plasmonic systems to geometrical changes, the influence of subtle chemical changes cannot be neglected. The data presented here demonstrates that chemical composition has a more pronounced effect than previously thought. This may occur via properties beyond refractive index and conductance, where such properties are relevant at this few-molecule sub-nm scale. The combination of molecular spacers, the tuning of their electronic states, and well-defined metallic architectures points to the clear need for improved theory combining molecules and plasmonics.

Conclusion

A sub-nm plasmon ruler with unprecedented sub-Å fine-control of gap size is assembled experimentally using rare-earth bis-phthalocyanine derivatives with different metal centres in a nanoparticle-on-mirror system. The small gap size produces highly red-shifted coupled modes, with large field enhancements that result in very large SERS enhancements. An anomalously large spectral shift is observed as the size of the central Ln ion is varied, with a magnitude unable to be predicted by local numerical or analytical models. Effects of tuning in molecular properties and structure are found unable to explain the data, instead leading to reduction of predicted tuning rates. These gap spacings are well within the nonlocal regime and small enough that quantum tunnelling effects are expected to be non-negligible. However, current understandings of quantum corrections to these plasmonic systems also give a reduction rather than an enhancement in the tuning rate with decreasing gap size, against what is observed. We emphasise that the data presented here is reproducible across thousands of individual NPoMs and multiple sample preparations. We speculate that coupling of conjugated organic π-systems with electrons in the nearby Au across a wide range of wavevectors leads to subtle changes in the quantum tunnelling dependence and the plasmonic tuning. It is also likely that that the understanding of refractive index is no longer possible as a continuum complex variable at this atomic scale. New treatments of light at the sub-nanometre scale are thus demanded.

Materials & Methods:

BPc* synthesis: BPc* compounds were synthesised according to a two-step procedure adapted from that of Ban et al.[64]

4,5-Bis(dodecylthio)phthalonitrile: 4,5-dichlorophthalonitrile (5.295 g, 26.88 mmol) and 1-dodecanethiol (15.5 mL, 64.7 mmol) were added to anhydrous DMSO (125 mL) and purged with N_2 at 100 °C, with stirring, for 15 min. Finely powdered anhydrous K_2CO_3 (35 g, 250 mmol) was added to the stirred reaction mixture in 7g portions every 5 min. The mixture was then stirred at 100 °C for a further 30 min. The red/brown mixture was cooled to room temperature, diluted with deionised water (300 mL) and extracted with $CHCl_3$ (5 × 100 mL). The combined organic extract was washed with deionised water (3 × 170 mL) and dried over $MgSO_4$. After removal of the solvent, the crude product was purified by column chromatography over silica gel [DCM/pet ether 60:40 (v/v)] and recrystallized twice from *n*-hexane to yield 4,5-bis(dodecylthio)phthalonitrile (11.62 g, 81.75%) as fluffy, off-white, plate-like crystals.

$LuPc^*_2$: A stirred mixture of 4,5-bis(dodecylthio)phthalonitrile (1.38 g, 2.61 mmol), lutetium acetate hydrate (0.137 g, 0.389 mmol) and 1,8-diazabicyclo[5.4.0]undec-7-ene (DBU) (0.143 mL, 0.956 mmol) in 1-hexanol (30 mL) was refluxed for 20 h under N_2 with molecular sieves. The dark green/black solution was cooled to room temperature and precipitated with MeOH. The waxy crude product was collected by vacuum filtration, washed with cold MeOH, purified three times by column chromatography [silica gel; DCM/petroleum ether (bpt 40-60 °C), 30:70 v/v] and recrystallized four times from ethyl acetate. The product was dried under high vacuum, with heating, to yield $LuPc^*_2$ (251 mg, 17.5%) as a waxy green/black solid. $ErPc^*_2$, $TbPc^*_2$ and $SmPc^*_2$ were prepared from the respective $Ln(OAc)_3$ precursors using the same method. See SI for full details and characterisation.

Sample Preparation: Template-stripped gold (TSG) substrates were prepared as follows: a Si wafer was cleaned with a Decon 90 solution and rinsed with isopropanol, ethanol and deionised water. Au was then evaporated at a rate of 1 Å s^{-1}, to a thickness of 200 nm. Small Si pieces (~1 cm^2) were attached to the exposed Au with Epo-Tek 377 epoxy resin, cured at 150 °C and cooled to room temperature gradually (0.5 °C/min) to minimise strain in the Au layer. Each substrate was lifted off immediately prior to each use to expose a clean Au surface. Fresh TSG samples were immersed in a 1 mM solution of BPc* in n-hexane. After 10 - 90 minutes, the TSG was removed, rinsed with n-hexane and dried with compressed N_2. Samples were exposed to AuNP solution (80 nm, citrate-capped) for 30 seconds, rinsed with distilled water and dried again with compressed N_2.

Darkfield Analysis: Individual NPoMs were illuminated with incoherent white light at an annular illumination angle (α) of 63-75°; scattered light was collected with an angle (β) of < 63°. A white scattering substrate was used as a reference. Automated data collection was performed using particle tracking code written in Python.[2] The program first identifies NPoMs within a given sample area for detailed optical analysis. To correct for chromatic aberration and different NPoM focal heights (z), multiple spectra are collected over a $\Delta z \approx 5$ µm range for each NPoM and appropriately combined. The optimum focal position for each wavelength is obtained by fitting a Gaussian function to the depth-dependent scattering intensity.

Computational Details: For full computational details, see SI. Geometry optimisations and polarisability calculations were performed for gas-phase $LnPc_2$ and $[LnPc_2]^-$. The effect of skew angle on polarisability and overall energy was explored. Finite-difference time-domain simulations were also used to calculate the expected far-field scattering mode spectra. The gap height was meshed with 24 cells to ensure that the plasmon was well resolved in the gap, while the meshing for the NP was 1nm. The spacer was modelled with refractive index n = 1.5. Semi-local analytical calculations were performed using the model formulated by Benz *et al*.[24]

ASSOCIATED CONTENT

Supporting Information. Additional computational details. Full synthesis/characterisation details. BPc* UV-Vis absorption spectra. Example STM image of $TbPc^*_2$ on Au.

AUTHOR INFORMATION

Corresponding Author

*E-mail: (J.J.B.) jjb12@cam.ac.uk; (O.A.S.) oas23@cam.ac.uk

Notes

The authors declare no competing financial interest.

ACKNOWLEDGMENT

We acknowledge funding from the EPSRC Cambridge NanoDTC, EP/L015978/1

References

(1) Ciracì, C.; Hill, R. T.; Mock, J. J.; Urzhumov, Y.; Fernández-Domínguez, A. I.; Maier, S. A.; Pendry, J. B.; Chilkoti, A.; Smith, D. R. *Science* **2012**, *337*, 1072–1074.

(2) de Nijs, B.; Bowman, R. W.; Herrmann, L. O.; Benz, F.; Barrow, S. J.; Mertens, J.; Sigle, D. O.; Chikkaraddy, R.; Eiden, A.; Ferrari, A.; et al. *Faraday Discuss.* **2015**, *178*, 185–193.

(3) Wang, H. *Sci. Rep.* **2018**, *8*, 9589.

(4) Kasera, S.; Biedermann, F.; Baumberg, J. J.; Scherman, O. A.; Mahajan, S. *Nano Lett.* **2012**, *12*, 5924–5928.

(5) Kasera, S.; Herrmann, L. O.; del Barrio, J.; Baumberg, J. J.; Scherman, O. A. *Sci. Rep.* **2014**, *4*.

(6) Sigle, D. O.; Kasera, S.; Herrmann, L. O.; Palma, A.; de Nijs, B.; Benz, F.; Mahajan, S.; Baumberg, J. J.; Scherman, O. A. *J. Phys. Chem. Lett.* **2016**.

(7) Di Martino, G.; Sonnefraud, Y.; Kéna-Cohen, S.; Tame, M.; Ozdemir, S. K.; Kim, M. S.; Maier, S. A. *Nano Lett.* **2012**, *12*, 2504–2508.

(8) Bozhevolnyi, S. I.; Volkov, V. S.; Devaux, E.; Laluet, J.-Y.; Ebbesen, T. W. *Nature* **2006**, *440*, 508.

(9) Ozbay, E. *Science* **2006**, *311*, 189–193.

(10) Zia, R.; Schuller, J. A.; Chandran, A.; Brongersma, M. L. *Mater. today* **2006**, *9*, 20–27.

(11) Reinhard, B. M.; Siu, M.; Agarwal, H.; Alivisatos, A. P.; Liphardt, J. *Nano Lett.* **2005**, *5*, 2246–2252.

(12) Jain, P. K.; Huang, W.; El-Sayed, M. A. *Nano Lett.* **2007**, *7*, 2080–2088.

(13) Ben, X.; Park, H. S. *J. Phys. Chem. C* **2011**, *115*, 15915–15926.

(14) Ben, X.; Park, H. S. *J. Phys. Chem. C* **2012**, *116*, 18944–18951.

(15) Hill, R. T.; Mock, J. J.; Hucknall, A.; Wolter, S. D.; Jokerst, N. M.; Smith, D. R.; Chilkoti, A. *ACS Nano* **2012**, *6*, 9237–9246.

(16) Dolinnyi, A. I. *J. Phys. Chem. C* **2015**, *119*, 4990–5001.

(17) Sönnichsen, C.; Reinhard, B. M.; Liphardt, J.; Alivisatos, A. P. *Nat. Biotechnol.* **2005**, *23*, 741.

(18) Lerch, S.; Reinhard, B. M. *Adv. Mater.* **2016**, *28*, 2030–2036.

(19) Lerch, S.; Reinhard, B. M. *Int. J. Mod. Phys. B* **2017**, *31*, 1740002.

(20) Hajisalem, G.; Min, Q.; Gelfand, R.; Gordon, R. *Opt. Express* **2014**, *22*, 9604–9610.

(21) Savage, K. J.; Hawkeye, M. M.; Esteban, R.; Borisov, A. G.; Aizpurua, J.; Baumberg, J. J. *Nature* **2012**, *491*, 574–577.

(22) Romero, I.; Aizpurua, J.; Bryant, G. W.; De Abajo, F. J. G. *Opt. Express* **2006**, *14*, 9988–9999.

(23) Myroshnychenko, V.; Rodríguez-Fernández, J.; Pastoriza-Santos, I.; Funston, A. M.; Novo, C.; Mulvaney, P.; Liz-Marzan, L. M.; de Abajo, F. J. G. *Chem. Soc. Rev.* **2008**, *37*, 1792–1805.

(24) Benz, F.; de Nijs, B.; Tserkezis, C.; Chikkaraddy, R.; Sigle, D. O.; Pukenas, L.; Evans, S. D.; Aizpurua, J.; Baumberg, J. J. *Opt. Express* **2015**, *23*, 33255–33269.

(25) Aubry, A.; Lei, D. Y.; Maier, S. A.; Pendry, J. B. *ACS Nano* **2011**, *5*, 3293–3308.

(26) David, C.; García de Abajo, F. J. *J. Phys. Chem. C* **2011**, *115*, 19470–19475.

(27) Dong, T.; Ma, X.; Mittra, R. *Appl. Phys. Lett.* **2012**, *101*, 233111.

(28) Teperik, T. V; Nordlander, P.; Aizpurua, J.; Borisov, A. G. *Opt. Express* **2013**, *21*, 27306–27325.

(29) Teperik, T. V; Nordlander, P.; Aizpurua, J.; Borisov, A. G. *Phys. Rev. Lett.* **2013**, *110*, 263901.

(30) Ciracì, C.; Urzhumov, Y.; Smith, D. R. *JOSA B* **2013**, *30*, 2731–2736.

(31) Zuloaga, J.; Prodan, E.; Nordlander, P. *Nano Lett.* **2009**, *9*, 887–891.

(32) Zhu, W.; Crozier, K. B. *Nat Commun* **2014**, *5*.

(33) Zhu, W.; Esteban, R.; Borisov, A. G.; Baumberg, J. J.; Nordlander, P.; Lezec, H. J.; Aizpurua, J.; Crozier, K. B. *Nat. Commun.* **2016**, *7*, 11495.

(34) Scholl, J. A.; García-Etxarri, A.; Koh, A. L.; Dionne, J. A. *Nano Lett.* **2013**, *13*, 564–569.

(35) David, C.; García de Abajo, F. J. *ACS Nano* **2014**, *8*, 9558–9566.

(36) Esteban, R.; Zugarramurdi, A.; Zhang, P.; Nordlander, P.; García-Vidal, F. J.; Borisov, A. G.; Aizpurua, J. *Faraday Discuss.* **2015**, *178*, 151–183.

(37) Esteban, R.; Borisov, A. G.; Nordlander, P.; Aizpurua, J. *Nat. Commun.* **2012**, *3*, 825.

(38) Halas, N. J.; Lal, S.; Chang, W.-S.; Link, S.; Nordlander, P. *Chem. Rev.* **2011**, *111*, 3913–3961.

(39) Berndt, R.; Gimzewski, J. K.; Schlittler, R. R. *Ultramicroscopy* **1992**, *42*, 355–359.
(40) Vilan, A.; Aswal, D.; Cahen, D. **2017**.
(41) Hajisalem, G.; Nezami, M. S.; Gordon, R. *Nano Lett.* **2014**, *14*, 6651–6654.
(42) Rousseau, R.; Aroca, R.; Rodriguez-Mendez, M. L. *J. Mol. Struct.* **1995**, *356*, 49–62.
(43) Koike, N.; Uekusa, H.; Ohashi, Y.; Harnoode, C.; Kitamura, F.; Ohsaka, T.; Tokuda, K. *Inorg. Chem.* **1996**, *35*, 5798–5804.
(44) Deng, Z.; Rauschenbach, S.; Stepanow, S.; Klyatskaya, S.; Ruben, M.; Kern, K. *Phys. Scr.* **2015**, *90*, 98003.
(45) Otsuki, J. *Supramol. Chem.* **2011**, *23*, 169–182.
(46) Miyake, K.; Fukuta, M.; Asakawa, M.; Hori, Y.; Ikeda, T.; Shimizu, T. *J. Am. Chem. Soc.* **2009**, *131*, 17808–17813.
(47) Qi, D.; Zhang, L.; Wan, L.; Zhang, Y.; Bian, Y.; Jiang, J. *Phys. Chem. Chem. Phys.* **2011**, *13*, 13277–13286.
(48) Bixner, O.; Lukeš, V.; Mančal, T.; Hauer, J.; Milota, F.; Fischer, M.; Pugliesi, I.; Bradler, M.; Schmid, W.; Riedle, E. *J. Chem. Phys.* **2012**, *136*, 204503.
(49) Prall, B. S.; Parkinson, D. Y.; Fleming, G. R.; Yang, M.; Ishikawa, N. *J. Chem. Phys.* **2004**, *120*, 2537–2540.
(50) Prall, B. S.; Parkinson, D. Y.; Ishikawa, N.; Fleming, G. R. *J. Phys. Chem. A* **2005**, *109*, 10870–10879.
(51) Komeda, T.; Isshiki, H.; Liu, J.; Zhang, Y.-F.; Lorente, N.; Katoh, K.; Breedlove, B. K.; Yamashita, M. *Nat. Commun.* **2011**, *2*, 217.
(52) Kahlal, S.; Mentec, A.; Pondaven, A.; L'Her, M.; Saillard, J.-Y. *New J. Chem.* **2009**, *33*, 574–582.
(53) Ishikawa, N.; Ohno, O.; Kaizu, Y.; Kobayashi, H. *J. Phys. Chem.* **1992**, *96*, 8832–8839.
(54) Mertens, J.; Eiden, A. L.; Sigle, D. O.; Huang, F.; Lombardo, A.; Sun, Z.; Sundaram, R. S.; Colli, A.; Tserkezis, C.; Aizpurua, J. *Nano Lett.* **2013**, *13*, 5033–5038.
(55) Maitrot, M.; Guillaud, G.; Boudjema, B.; André, J.-J.; Strzelecka, H.; Simon, J.; Even, R. *Chem. Phys. Lett.* **1987**, *133*, 59–62.
(56) Liu, Y.; Shigehara, K.; Hara, M.; Yamada, A. *J. Am. Chem. Soc.* **1991**, *113*, 440–443.
(57) Rodriguez-Mendez, M. L.; Aroca, R.; DeSaja, J. A. *Chem. Mater.* **1993**, *5*, 933–937.
(58) de Saja, J. A.; Rodríguez-Méndez, M. L. *Adv. Colloid Interface Sci.* **2005**, *116*, 1–11.
(59) Wulan, Q.; Kitamura, F. *Bull. Chem. Soc. Jpn.* **2007**, *80*, 1740–1745.
(60) Taylor, R. W.; Lee, T.-C.; Scherman, O. A.; Esteban, R.; Aizpurua, J.; Huang, F. M.; Baumberg, J. J.; Mahajan, S. *ACS Nano* **2011**, *5*, 3878–3887.
(61) Benz, F.; Tserkezis, C.; Herrmann, L. O.; de Nijs, B.; Sanders, A.; Sigle, D. O.; Pukenas, L.; Evans, S. D.; Aizpurua, J.; Baumberg, J. J. *Nano Lett.* **2015**, *15*, 669–674.
(62) Klymchenko, A. S.; Sleven, J.; Binnemans, K.; De Feyter, S. *Langmuir* **2006**, *22*, 723–728.
(63) Yang, Z.-Y.; Gan, L.-H.; Lei, S.-B.; Wan, L.-J.; Wang, C.; Jiang, J.-Z. *J. Phys. Chem. B* **2005**, *109*, 19859–19865.
(64) Ban, K.; Nishizawa, K.; Ohta, K.; van de Craats, A. M.; Warman, J. M.; Yamamoto, I.; Shirai, H. *J. Mater. Chem.* **2001**, *11*, 321–331.
(65) Akkerman, H. B.; Blom, P. W. M.; De Leeuw, D. M.; De Boer, B. *Nature* **2006**, *441*, 69.
(66) Byers, C. P.; Hoener, B. S.; Chang, W.-S.; Yorulmaz, M.; Link, S.; Landes, C. F. *J. Phys. Chem. B* **2014**, *118*, 14047–14055.
(67) Robaschik, P.; Fronk, M.; Toader, M.; Klyatskaya, S.; Ganss, F.; Siles, P. F.; Schmidt, O. G.; Albrecht, M.; Hietschold, M.; Ruben, M. *J. Mater. Chem. C* **2015**, *3*, 8039–8049.
(68) Seidel, F.; Fronk, M.; Himcinschi, C.; Chis, V.; Zahn, D. R. T. *Phys. status solidi* **2010**, *7*, 222–226.
(69) Katoh, K.; Yoshida, Y.; Yamashita, M.; Miyasaka, H.; Breedlove, B. K.; Kajiwara, T.; Takaishi, S.; Ishikawa, N.; Isshiki, H.; Zhang, Y. F.; et al. *J. Am. Chem. Soc.* **2009**, *131*, 9967–9976.
(70) Glebe, U.; Weidner, T.; Baio, J. E.; Schach, D.; Bruhn, C.; Buchholz, A.; Plass, W.; Walleck, S.; Glaser, T.; Siemeling, U. *Chempluschem* **2012**, *77*, 889–897.
(71) Siemeling, U.; Schirrmacher, C.; Glebe, U.; Bruhn, C.; Baio, J. E.; Árnadóttir, L.; Castner, D. G.;

Weidner, T. *Inorganica Chim. Acta* **2011**, *374*, 302–312.
(72) Chikkaraddy, R.; de Nijs, B.; Benz, F.; Barrow, S. J.; Scherman, O. A.; Rosta, E.; Demetriadou, A.; Fox, P.; Hess, O.; Baumberg, J. J. *Nature* **2016**, *535*, 127.
(73) de la Torre, G.; Claessens, C. G.; Torres, T. *Chem. Commun.* **2007**, No. 20, 2000–2015.
(74) Yoshino, K.; Lee, S. B.; Sonoda, T.; Kawagishi, H.; Hidayat, R.; Nakayama, K.; Ozaki, M.; Ban, K.; Nishizawa, K.; Ohta, K. *J. Appl. Phys.* **2000**, *88*, 7137–7143.
(75) Ishikawa, N.; Sugita, M.; Okubo, T.; Tanaka, N.; Iino, T.; Kaizu, Y. *Inorg. Chem.* **2003**, *42*, 2440–2446.
(76) Fu, Y.-S.; Schwöbel, J.; Hla, S.-W.; Dilullo, A.; Hoffmann, G.; Klyatskaya, S.; Ruben, M.; Wiesendanger, R. *Nano Lett.* **2012**, *12*, 3931–3935.
(77) Hückstädt, H.; Tutaß, A.; Göldner, M.; Cornelissen, U.; Homborg, H. *Zeitschrift für Anorg. und Allg. Chemie* **2001**, *627*, 485–497.
(78) Vitali, L.; Fabris, S.; Conte, A. M.; Brink, S.; Ruben, M.; Baroni, S.; Kern, K. *Nano Lett.* **2008**, *8*, 3364–3368.
(79) Pan, Y.; Kanisawa, K.; Ishikawa, N.; Fölsch, S. *J. Phys. Condens. Matter* **2017**, *29*, 364001.
(80) Noda, Y.; Noro, S.; Akutagawa, T.; Nakamura, T. *Sci. Rep.* **2014**, *4*, 3758.
(81) Toscano, G.; Straubel, J.; Kwiatkowski, A.; Rockstuhl, C.; Evers, F.; Xu, H.; Mortensen, N. A.; Wubs, M. *Nat. Commun.* **2015**, *6*, 7132.
(82) Garcia de Abajo, F. J. *J. Phys. Chem. C* **2008**, *112*, 17983–17987.
(83) Luo, Y.; Fernandez-Dominguez, A. I.; Wiener, A.; Maier, S. A.; Pendry, J. B. *Phys. Rev. Lett.* **2013**, *111*, 93901.